Journal of Fluids and Structures 42 (2013) 25–39

Contents lists available at ScienceDirect

Journal of Fluids and Structures

journal homepage: www.elsevier.com/locate/jfs

Suppression of vortex-induced vibration of a circular cylinder using suction-based flow control

Wen-Li Chen [a,b,*], Da-Bo Xin [a], Feng Xu [c], Hui Li [a], Jin-Ping Ou [a,d], Hui Hu [b]

[a] School of Civil Engineering, Harbin Institute of Technology, Harbin 150090, China
[b] Department of Aerospace Engineering, Iowa State University, Ames, IA 50011, USA
[c] School of Civil and Environment Engineering, Harbin Institute of Technology Shenzhen Graduate School, Shenzhen 518055, China
[d] School of Civil and Hydraulic Engineering, Dalian University of Technology 116024, China

ARTICLE INFO

Article history:
Received 4 February 2012
Accepted 13 May 2013
Available online 19 June 2013

Keywords:
Flow around a circular cylinder
Vortex-induced vibration
Flow control
Steady suction
Mitigation of vortex-induced vibration

ABSTRACT

In the present study, a flow control method is employed to mitigate vortex-induced vibration (VIV) of a circular cylinder by using a suction flow method. The VIV of a circular cylinder was first reproduced in a wind tunnel by using a spring–mass system. The time evolution of the cylinder oscillation and the time histograms of the surface pressures of 119 taps in four sections of the circular cylinder model were measured during the wind tunnel experiments. Four steady suction flow rates were used to investigate the effectiveness of the suction control method to suppress VIV of the circular cylinder. The vibration responses, the mean and fluctuating pressure coefficients, and the resultant aerodynamic force coefficients of the circular cylinder under the suction flow control are analyzed. The measurement results indicate clearly that the steady suction flow control method exhibits excellent control effectiveness and can distinctly suppress the VIV by dramatically reducing the amplitudes of cylinder vibrations, fluctuating pressure coefficients and lift coefficients of the circular cylinder model. By comparing the test cases with different suction flow rates, it is found that there exists an optimal suction flow rate for the maximum VIV control. The cases with higher suction flow rates do not necessarily behave better than those with lower suction flow rates. With the experimental setting used in the present study, the suction flow control method is found to behave better for VIV suppression when the ratio of the suction flow velocity to the oncoming flow velocity is less than one.

1. Introduction

In recent years, long-span suspension bridges and cable-stayed bridges have been widely constructed worldwide due to their superior structural performance and elegant appearance. The key components of cable-stayed bridges, inclined cables, often vibrate under wind and rain, which are usually referred as vortex-induced vibration (VIV) (Main and Jones, 1999; Matsumoto et al., 2003; Zuo et al., 2008; Zuo and Jones, 2010) and rain-wind induced vibration (RWIV) (Hikami and Shiraishi, 1988), respectively. Although the VIV of the cables is self-limiting, it frequently occurs at low wind speeds. Frequent wind-induced vibration may induce fatigue damage to the cables. Therefore it is highly desirable to reduce the wind-induced vibrations for the optimized design and durability of the cable-stayed bridges. Besides using field measurements to monitor the VIV of full-scale cables on cable-stayed bridges (Zuo and Jones, 2010; Zuo et al., 2008),

* Corresponding author at: School of Civil Engineering, Harbin Institute of Technology, 73 Huanghe Road, Nan-gang District, Harbin, Heilongjiang 150090, China. Tel./fax: +86 451 86282068.
E-mail address: cwl_80@hit.edu.cn (W.-L. Chen).

0889-9746/$ - see front matter © 2013 Elsevier Ltd. All rights reserved.
http://dx.doi.org/10.1016/j.jfluidstructs.2013.05.009

a number of laboratory studies have also been conducted in recent years with finite segment cable models (i.e., cylinder models) to investigate the VIV phenomena and explore effective strategies to suppress the VIV of bridge cables. For examples, Farivar (1981), Sakamoto and Arie (1983), Baban and So (1991) and Zdravkovich et al. (1989) carried out laboratory experiments to quantify the vibration responses and flow characteristics around cylindrical stay cable models of finite lengths.

Viscous damper devices have been widely used to control the VIV and RWIV of stay cables of cable-stayed bridges (Main and Jones, 2001; Persoon and Noorlander, 1999; Zhou and Xu, 2007). Main and Jones (2001) found an additional optimal damping ratio to the stay cable provided by the viscous damper. Wang and Xu (2007) employed an active stiffness control method to suppress the RWIVs of prototype stay cables. Li et al. (2007) and Liu et al. (2007) investigated the theory, algorithm and model test of the semi-active control of stay cables' wind-induced vibrations using magnetorheological fluid dampers, which can effectively reduce the cable vibrations and increase the stay cables' system damping ratios. Instead of controlling/suppressing the VIVs, an interesting idea has also been suggested recently to try to harvest wind energy from the VIVs. Bernitsas et al. (2008) designed a vortex induced vibration aquatic clean energy (VIVACE) converter. The VIVACE was based on the idea of maximizing (rather than spoiling) vortex shedding and exploiting (rather than suppressing) VIV. It introduced optimal damping for energy conversion while maintaining VIV over a broad range of vortex shedding synchronization.

While the control mechanisms of each type of damper device described above provided additional damping to the stay cables and increased their ability to resist wind-induced vibrations, those methods did not change or reduce the wind loads on the stay cables. Aerodynamic methods, including passive and active control approaches, can be used to reduce the wind loads on the stay cables. These methods can also increase the natural damping ratio of the stay cables. Matsumoto et al. (1992) and Flamand (1995) proposed the use of protuberances to suppress the RWIVs of stay cables. Gu and Du (2005) conducted wind tunnel tests using double-spiral wires to mitigate vibration. Owen and Bearman (2001) attached hemispherical bumps to the circular cylinder surface to control the vortex-induced vibration amplitudes of the cable models. Bao and Tao (2013) employed dual parallel plates which were symmetrically attached at the rear surface to control the wake flow of a circular cylinder. Oruç (2012) carried out a passive control for the flow structures around a circular cylinder by using a streamline screen which surrounded the circular cylinder. Wu et al. (2012) performed an experimental study on the suppression the VIV of a long flexible riser by using multiple control rods.

Many active flow approaches were also used to control the flow separation and flow-induced vibration. Wu et al. (2007) developed a moving-wall control strategy, e.g., appropriate traveling transverse wave, to manage the unsteady separated flow over a circular cylinder. This method allows the global flow to remain attached when there is a strong adverse pressure gradient and eliminates vortex shedding. Modi (1997), Munshi et al. (1997), Patnaik and Wei (2002) and Korkischko and Meneghini (2012) used momentum injections to control the flow field around the airfoils, flat plates, rectangular prisms, D-section prisms and circular cylinders; they found that the momentum injection method could effectively resist the wind-induced vortex and galloping instabilities. Grager et al. (2011) used a dynamic burst control plate to suppress the stall on an airfoil by preventing the low-Reynolds-number leading edge separation bubble from bursting. Tchieu and Leonard (2012) employed synthetic jet actuators to control the flow structures around an airfoil. Feng et al. (2010, 2011) and Feng and Wang (2010) conducted a series of experimental studies to investigate the effects of a synthetic jet on the unsteady vortex shedding in the wake of a circular cylinder. They reported that the synthetic jet positioned at the rear stagnation point of the cylinder would generate a vortex pair, which could have a significant influence on the vortex shedding modes in the wake of the circular cylinder.

Suction flow controls have been widely used to suppress the flow separation of airfoils (Qin et al., 1998; Greenblatt et al., 2006; Gbadebo et al., 2008; Chng et al., 2009), plates (Arcas and Redekopp, 2004Fransson and Alfredsson, 2003; Seal and Smith 1999) and circular cylinders (Delaunay and Kaiktsis, 2001; Fransson et al., 2004; Li et al., 2003; Patil and Ng, 2010). Delaunay and Kaiktsis (2001) studied the effects of base suction and blowing on the stability and dynamics of the flow around a circular cylinder at low Reynolds numbers ($Re <= 90$). Slight blowing can stabilize the wake and reduce absolute instability in the near wake; a high enough suction can also stabilize the wake at $Re > 47$. Li et al. (2003) performed a complete control of vortex shedding with Reynolds numbers up to 110 via flow suction/blowing based on numerical simulations. It was observed that a short time window of flow control may suffice to suppress vortex shedding. Fransson et al. (2004) and Patil and Ng (2010) investigated suction flow control based on porosity of the entire or partial surface. The suction flow control has been found to lead to drag reduction, suppress the spanwise vortices formation, reduce the velocity fluctuation level and eliminate the oscillation of the lift.

In this paper, a steady suction flow control method is adopted to mitigate the VIV of a circular cylinder. The context of the present study is arranged as follows. In Section 2, a wind tunnel test for the VIV of a circular cylinder was set up in order to assess the effectiveness of using the suction control system for VIV suppression. In Sections 3–5, the measurement results in terms of the cylinder oscillations, pressure distributions and aerodynamic forces acting on the circular cylinder without suction flow control are analyzed and discussed. The measurement results with suction flow control are discussed in Section 6, followed by a section of conclusions derived from the present study.

2. Experiment set-up

The experimental study was performed in the Joint Laboratory of Wind Tunnel and Wave Flume located at the Harbin Institute of Technology as shown in Fig. 1. The wind tunnel is a closed loop tunnel with two test sections. The dimension of

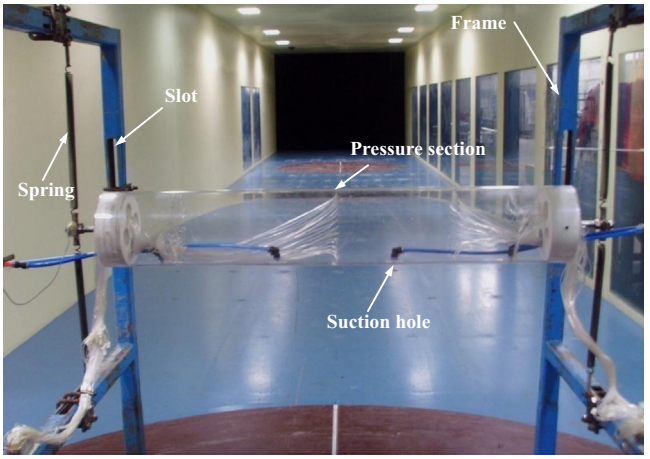

Fig. 1. Experimental setup to study the VIV of a cylindrical cable model.

the smaller test section is 4.0 m (width) × 3.0 m (height) with a length of 25 m, and that of the larger section is 6.0 m (width) × 3.6 m (height) with a length of 50 m. The wave trough is located under the larger test section and separated by movable floors. The maximum wind speeds can be up to 50 m/s and 30 m/s for the smaller and larger test sections, respectively.

2.1. Circular cylinder model

The cylindrical cable model used in the present study was made of an acrylic resin pipe with a length L of 1.2 m, a diameter D of 0.2 m and a wall thickness of 6 mm. The weight of the cylinder model per unit length was 8.71 kg/m. The vortex-induced vibration of the circular cylinder model was produced by using a spring–mass system. The cylinder model was suspended by two springs at two ends in the cross-flow direction, as shown in Fig. 1. The height of the axis of the cylinder model was set at 1.2 m above the wind tunnel floor, and the yaw angle with respect to the oncoming wind and the inclined angle of the cylinder model were set to zero in the present study. Two accelerometers (Brüel and Kjær 4507B) were mounted at the ends of the test model in the cross-wind direction to collect the vibration signals. The sampling rate was set of 1000 Hz, and the sampling time was 100 s. Prior to the wind tunnel tests, free vibration tests were conducted to obtain the damping ratio and natural frequency of the spring–mass system in the cross flow direction, which were determined to be 0.63% and 5.61 Hz (i.e., $f_0 = 5.61$ Hz), respectively.

A digital pressure measurement system (model DSM3400; Scanivalve Corporation) was used in the present study to measure the surface pressure distributions on the cylindrical cable model. One-hundred and nineteen pressure taps were arranged on the test model in four sections, with 30 taps each for the three left sections and 29 taps for the right section (one tap was replaced by a suction hole), as shown in Fig. 2(a) and (b). The sampling rate and sampling time for the pressure measurements were set to be 312.5 Hz and 100 s, respectively. In the present study, all the pressure taps were connected by using polyvinyl chloride (PVC) tubes of 1.35 m length to the digital pressure measurement system. In order to correct the amplitude attenuation and phase lag of the pressure signals caused by the 1.35 m long PVC tubes for the quantitative pressure measurements, the characteristics of the measured pressure values through the PVC tubes were calibrated in advance with a low-frequency wave generator. The calibrated frequencies were up to 300 Hz, which is significantly higher than the dominant frequency of the VIV for the present study (i.e., 5.61 Hz). Then, the measured pressure data were corrected by using the calibration results. Further information about the calibration procedure and results is available at Qiu (2010). The mean and fluctuating pressure coefficients and the aerodynamic force coefficients (C_x and C_y) given in the present study are the values obtained after performing the correction procedure.

2.2. Suction flow control system and studied cases

As shown in Figs. 1 and 2, four suction holes with a diameter of 10 mm were located on the lowest positions of the circular cylinder at a spacing of 300 mm. One end of a suction pipe was linked to a suction hole, and the other end was connected to a suction pump system. The outer and inner diameters of the suction pipe were 10 mm and 7.5 mm, respectively. The flow rate of each suction pipe could be individually adjusted by using the control valves installed on the suction pipes according to the wind tunnel test requirements.

The suction flow velocities through the holes were important flow control parameters and were determined based on the bulk flow rates and inner diameter of the suction pipes. To investigate the control effectiveness at different suction flow velocities, the following five flow rates for each suction pipe were used in the present study: 0, 10, 13, 16 and 19 l/min. The flow rates of the four suction holes were set to be the same for all of the test cases. The mean suction flow velocities $\overline{U}_{suc}$

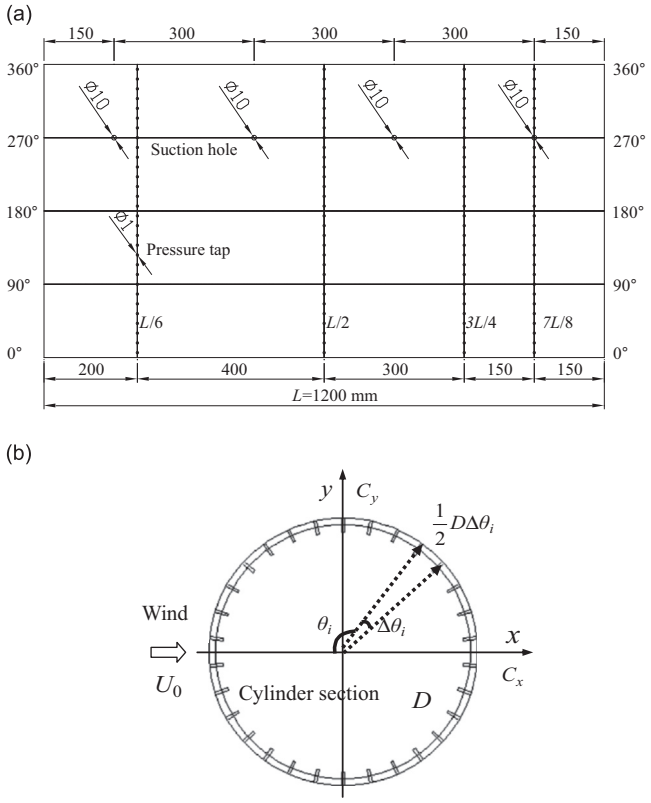

Fig. 2. Pressure tap and suction hole arrangements: (a) pressure taps in four sections and the four suction hole locations; (b) arrangement of the pressure taps in each section.

Table 1
Test cases and corresponding suction flow velocities and suction momentum coefficients.

Cases/flow rate (liter/min)	0	10	13	16	19
Suction velocity (m/s)	0	3.773	4.904	6.036	7.168
Suction momentum coefficient	0	0.00048∼0.0014	0.00081∼0.0023	0.0012∼0.0035	0.0017∼0.0049

Note: U_0=5.24–8.85 m/s.

through the suction holes corresponding to each test case are listed in Table 1. Following the work of Amitay et al. (1997, 1998) and Tensi et al. (2002), suction momentum coefficient, which represents the ratio of the suction momentum flux to the oncoming free-stream momentum flux, is used as the non-dimensional parameter to characterize the test cases with suction flow control. In the present study, the suction momentum coefficient is defined as

$$C_\mu = 2\left(\frac{\overline{U}_{\text{suc}}}{U_0}\right)^2\left(\frac{4S_{\text{suc}}}{DL}\right), \tag{1}$$

where S_{suc} is the section area of each suction hole, $L/4$ is the space between two neighboring suction holes, U_0 is the oncoming velocity of free streams changing from 5.24 to 8.85 m/s. The suction momentum coefficients C_μ corresponding to each test case are also listed in Table 1.

3. Cylinder model response

3.1. No control

The vibrations of the cylinder model were first measured without suction flow control at the following 13 wind speeds in the range of 5.24–8.85 m/s. The corresponding reduced velocities, which is defined as U_0/f_0D, are in the range of 4.67–7.89, respectively. The cross-flow amplitudes of the VIV of the test model, presented as the ratios of vibration amplitudes A to the model diameter D, versus reduced velocity are shown in Fig. 3. It can be seen clearly that the VIV of the test model would occur with the reduced velocity in the range of 5.45–6.86. It should be noted, the VIV amplitude of a circular cylinder in

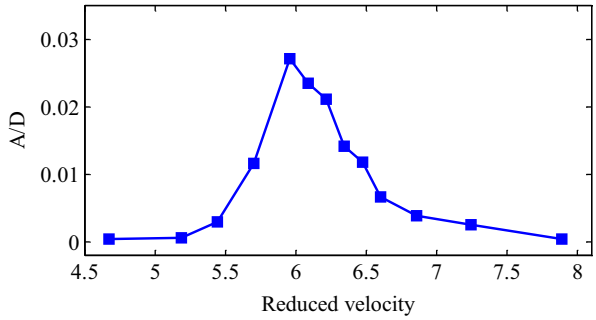

Fig. 3. Oscillation amplitudes of the VIV versus reduced velocity.

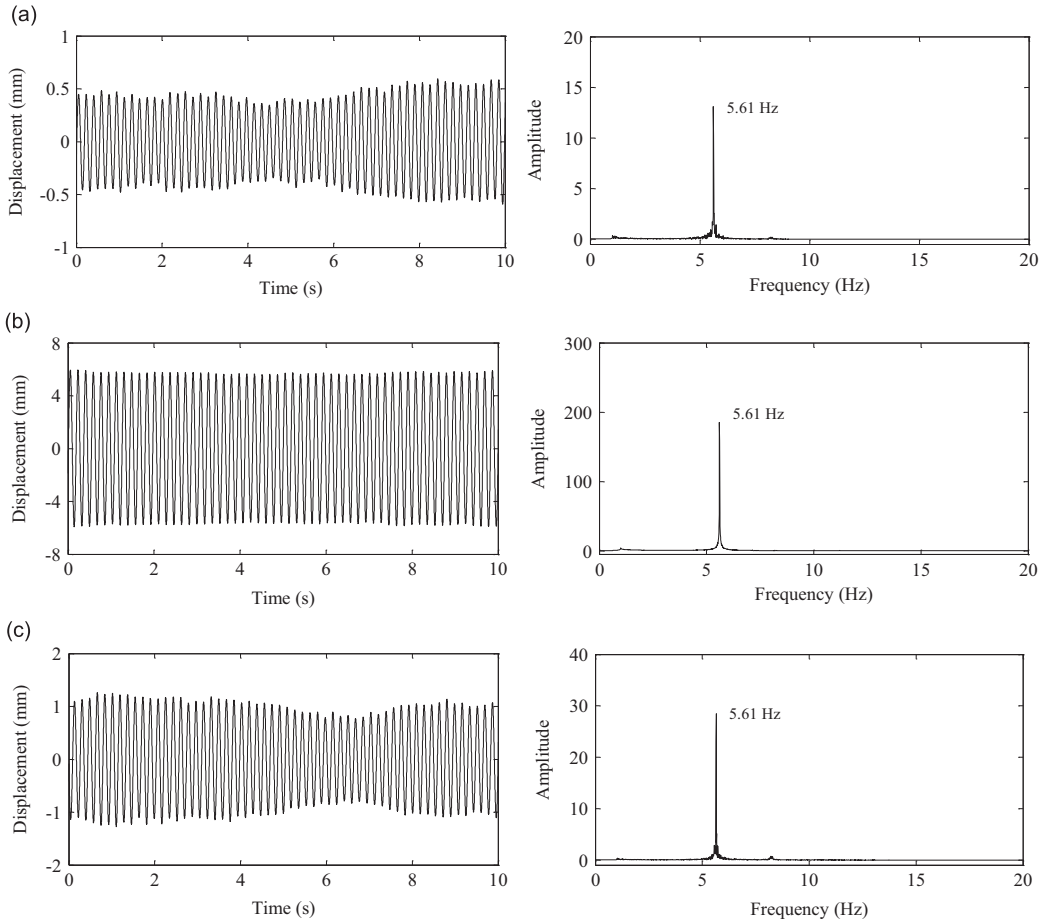

Fig. 4. Time histories and frequency spectra of the cross-flow vibrations of the test model at different reduced velocities: (a) 5.45, (b) 5.96 and (c) 6.86.

airflow (i.e., the test cases of the present study) would be much smaller compared with those in water in general due to a much larger reduced damping, S_G, in airflow. It is believed to be closely related to the large mass ratio of the test model in airflow, as suggested by Skop and Balasubramanian (1997).

The VIV time histories of the test model at the reduced velocities of 5.45, 5.96 and 6.86 which are corresponding to the VIV starting reduced velocity, the reduced velocity with the maximum VIV amplitude, and the VIV ending reduced velocity of the test model, respectively, are shown in Fig. 4(a) – (c). It can be seen clearly that, at the reduced velocity of 5.96 (i.e., the reduced velocity with the maximum VIV amplitude), the vibration of the test model is found to be quite steady with a well-defined dominant frequency of 5.61 Hz. It should be noted that the frequency of 5.61 Hz is the natural frequency of the test model. At the starting and ending reduced velocities of 5.45 and 6.86, while the vibration was found to have the same dominant frequency of 5.61 Hz, the amplitude of the oscillation is found to become much smaller and time-varying, compared with those at the reduced velocity of 5.96 with the maximum VIV amplitude.

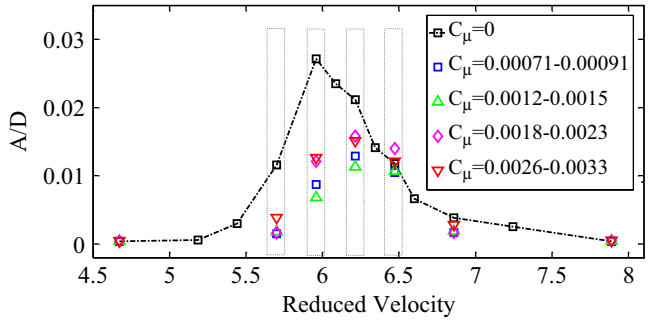

Fig. 5. Cross-flow oscillation amplitudes of the VIV versus reduced velocity.

Table 2
Test cases and corresponding suction momentum coefficients.

Flow rate (liter/min)	Reduced velocity				
	0	10	13	16	19
5.70	0	0.00091	0.0015	0.0023	0.0033
5.96	0	0.00083	0.0014	0.0021	0.0030
6.21	0	0.00077	0.0013	0.0020	0.0028
6.47	0	0.00071	0.0012	0.0018	0.0026

3.2. Suction control

The steady suction method was then used to control the VIV of the test model. Seven different suction flow velocities were tested in the present study, and the corresponding vibration amplitudes of the VIV are shown in Fig. 5. For the vibration, pressure and aerodynamic forces analysis with the suction flow control, focus was placed on the four cases with the reduced velocities of 5.70, 5.96, 6.21 and 6.47 because the vibration amplitudes are large at these values. The corresponding suction momentum coefficients at each suction flow rate and reduced velocity are listed in Table 2.

Time histories of the VIV displacements of the test model at the four reduced velocities adopting different suction flow velocities are shown in Fig. 6. The results with and without suction flow control are represented by the black and red dashed lines, respectively. At the reduced velocities of 5.70 and 5.96, the control effectiveness by using the suction flow approach was evident as the VIV amplitudes of the four suction velocities were reduced by at least 50%. At the reduced velocities of 6.21, the cases with suction rates of 16 ($C_\mu = 0.0020$) and 19 l/min ($C_\mu = 0.0028$) are found to have less control effectiveness. At the reduced velocities of 6.47, the cases with suction rates from 13 to 19 l/min (i.e.,$C_\mu = 0.0012$–0.0026) are found to have no control effectiveness; in particular, the case with the suction rate of 16 l/min ($C_\mu = 0.0018$) is found to enlarge the VIV amplitude of the cylinder model at the reduced velocity of 6.47.

According to these results, the VIV amplitude is found to be reduced most significantly for the case with the suction rate of 13 l/min ($C_\mu = 0.0012$–0.0015), followed by the case with the suction rate of 10 l/min ($C_\mu = 0.00071$–0.00091), and then the cases with suction rates of 16 ($C_\mu = 0.0018$–0.0023) and 19 l/min ($C_\mu = 0.0026$–0.0033), as shown in Fig. 7.

4. Pressure coefficients of the cylinder model

4.1. No control

The time histories of the measured surface pressure distribution on the test model were first measured without applying the suction flow control. As the wind speed increases, the VIV appears, reaches its maximum oscillation amplitude, and then disappears, as shown in Fig. 3. The mean pressure coefficients in the positive regions remain fairly constant during this process, but the absolute values of the mean pressure coefficients in the negative regions are found to increase, reach their maximum values, and then decrease, as shown in Fig. 8. The cylinder vibration increases the fluctuating pressures on the circular cylinder's surface, and the increased fluctuating pressures promote the vibration of the test model. The vibration and fluctuating pressure distribution reach maximum amplitude at the reduced velocity of 5.96. At the other reduced velocities, the fluctuating pressure distributions are found to be quite similar.

4.2. Suction control

The mean and fluctuating pressure distributions on the circular cylinder were then investigated for the VIV suppression of the test model with suction flow control. The results at the reduced velocity of 5.96 are shown in Fig. 9. For the mean

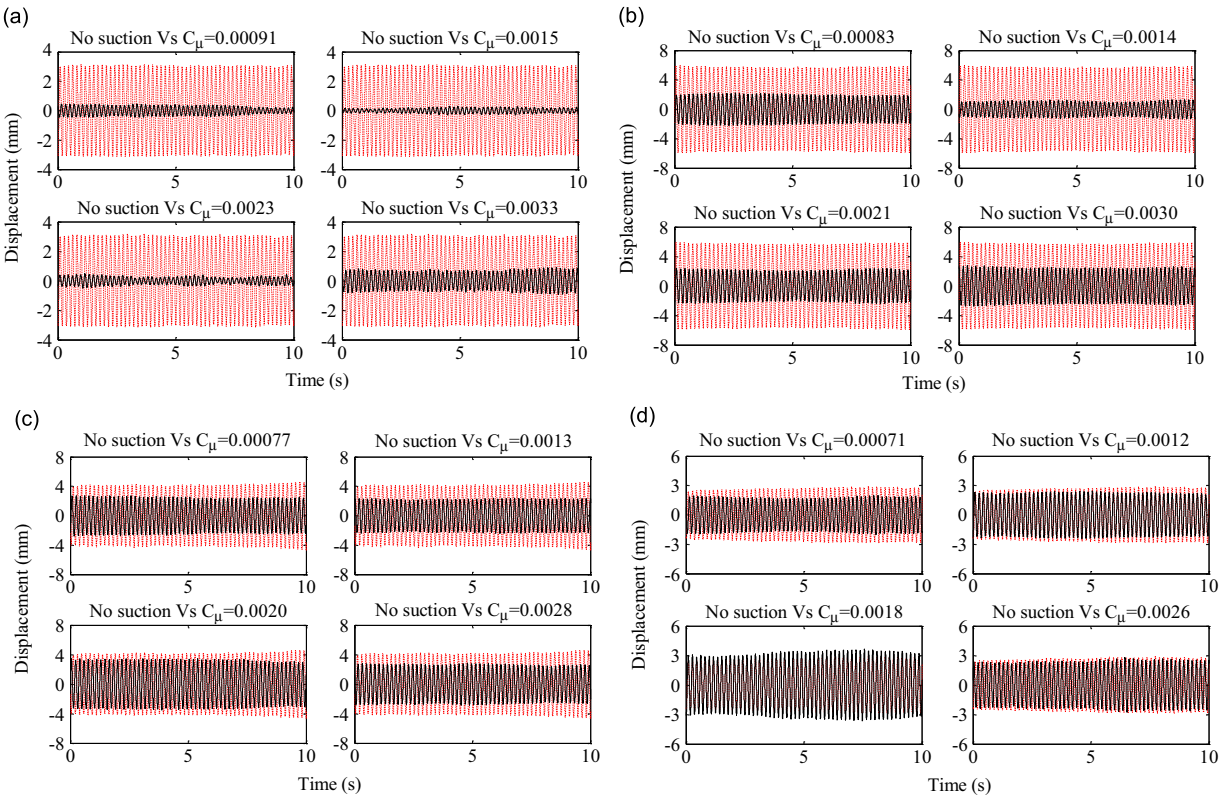

Fig. 6. Time histories and frequency spectra of the cross-flow vibrations of the test model at different reduced velocities: (a) 5.70, (b) 5.96, (c) 6.21 and (d) 6.47; the red lines denote the cases without suction control and the black lines denote those with suction control. (For interpretation of the references to color in this figure caption, the reader is referred to the web version of this article.)

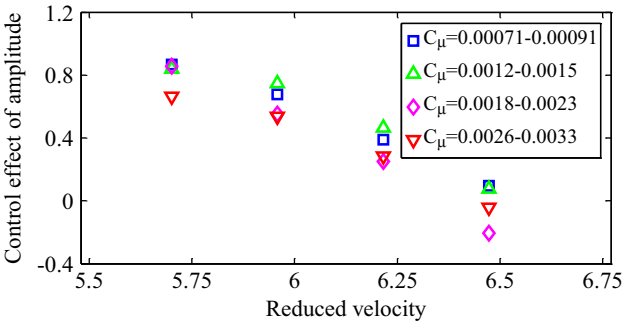

Fig. 7. VIV amplitudes of the test model vs. reduced velocity with suction flow control.

pressure coefficient distributions, the mean pressure coefficients in the positive regions remain fairly constant under the suction flow control, and the absolute values of the mean pressure coefficients in the negative regions are found to be decreased greatly in the cross sections of the $L/2$, $3L/4$ and $7L/8$. In the region around the suction hole at the $L/6$ section, the absolute values of the mean pressure coefficients are found to increase for the cases with the suction rates of 16 ($C_\mu = 0.0021$) and 19 l/min ($C_\mu = 0.0030$), as shown in left column of Fig. 9(a).

The suction dramatically decreases the fluctuating pressures at the $L/2$, $3L/4$ and $7L/8$ sections. However, in the region around the suction hole at the $L/6$ section, the test cases with suction rates of 16 ($C_\mu = 0.0021$) and 19 l/min ($C_\mu = 0.0030$) see significant increase in the fluctuating pressures. The difference between the results of the $L/6$ section and the other three sections need to be further investigated. This difference may be the reason for which the control effects of these two suction cases (i.e., with the suction flow rates of 16 ($C_\mu = 0.0021$) and 19 l/min ($C_\mu = 0.0030$)) are not as good as those of the other test cases (i.e., with the suction flow rates of 10 l/min ($C_\mu = 0.00083$) and 13 l/min ($C_\mu = 0.0014$)).

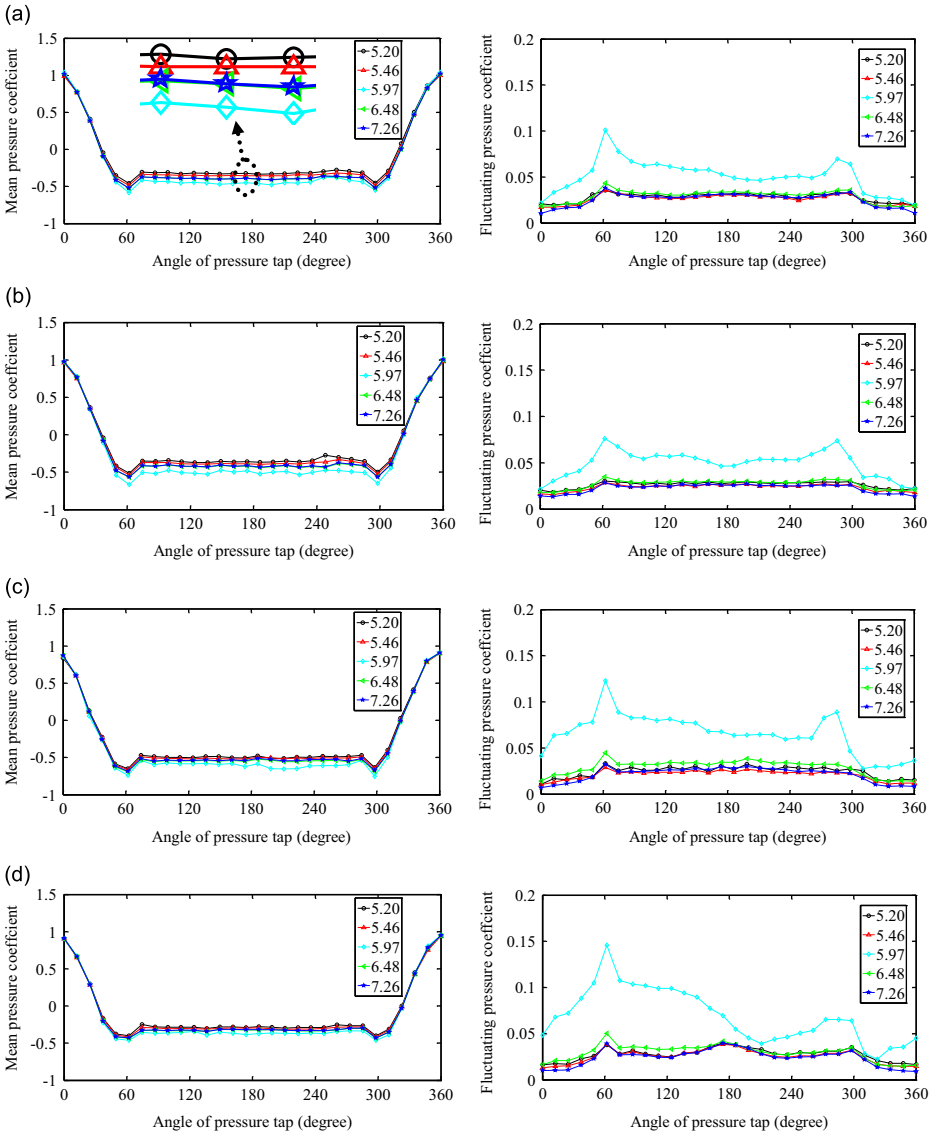

Fig. 8. Mean and fluctuating pressure distributions at different sections of the test model: (a) $L/6$, (b) $L/2$, (c) $3L/4$ and (d) $7L/8$.

5. Aerodynamic coefficients of the cylinder model

5.1. No control

A schematic of the model coordinate system and the directions of the aerodynamic coefficients are shown in Fig. 2(b). The x-coordinate is along the oncoming flow direction, and the y-coordinate is perpendicular to the oncoming flow direction. The aerodynamic coefficients can be obtained by integrating the wind pressures over all of the taps; the lift and drag coefficients, C_y and C_x, can then be calculated with the following expression:

$$C_x = \frac{F_x}{1/2\rho U_0^2 D} = \frac{1/2\rho U_0^2 \sum_i C_{p_i} \cdot 1/2D\Delta\theta_i \cdot \cos\theta_i}{1/2\rho U_0^2 D} = \frac{1}{2}\sum_i C_{p_i} \cdot \Delta\theta_i \cdot \cos\theta_i,$$

$$C_y = \frac{F_y}{1/2\rho U_0^2 D} = \frac{1/2\rho U_0^2 \sum_i C_{p_i} \cdot \frac{1}{2} D\Delta\theta_i \cdot \sin\theta_i}{1/2\rho U_0^2 D} = \frac{1}{2}\sum_i C_{p_i} \cdot \Delta\theta_i \cdot \sin\theta_i,$$

$$C_{p_i} = \frac{p_i - p_\infty}{1/2\rho U_0^2}, \tag{2}$$

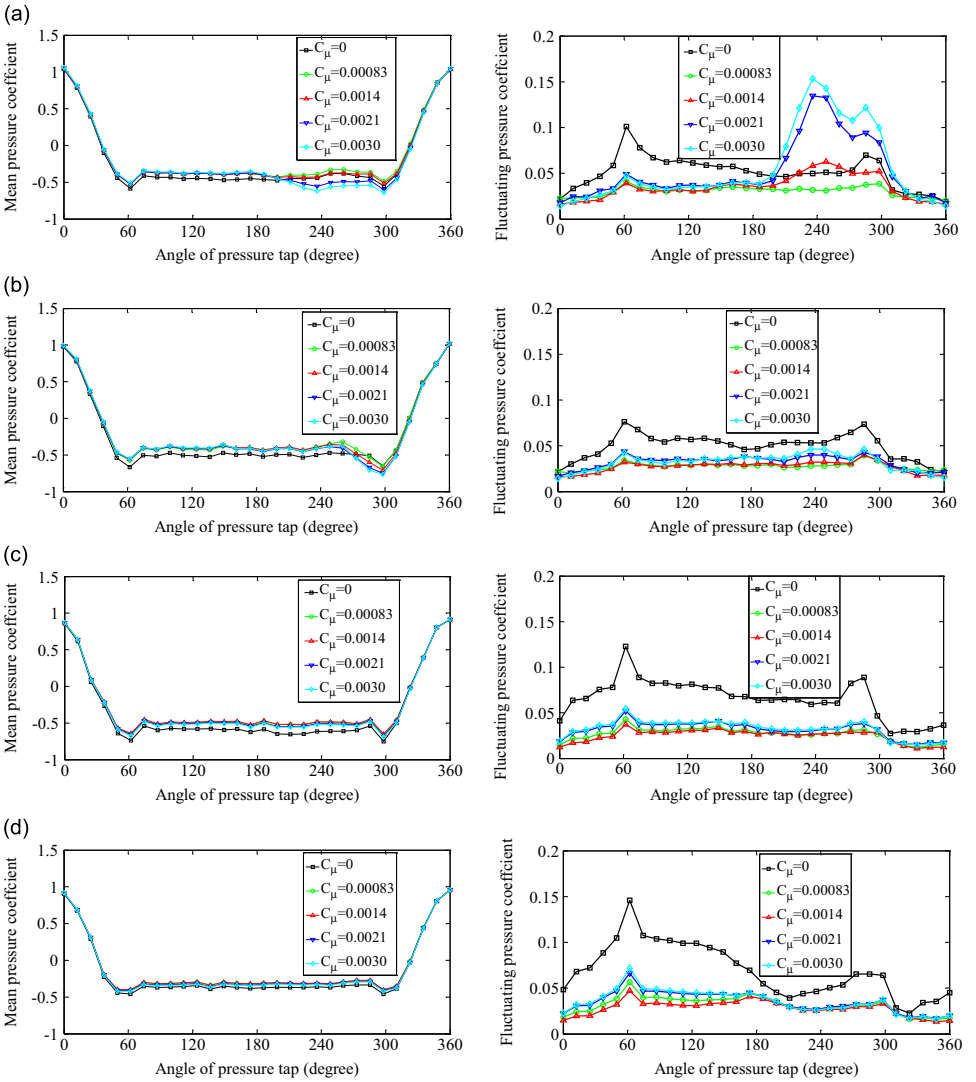

Fig. 9. Mean and fluctuating pressure distribution at different sections of the test model at a reduced velocity of 5.96 with suction control: (a) $L/6$, (b) $L/2$, (c) 3 $L/4$ and (d) 7 $L/8$.

where ρ is the air density, which is 1.225 kg/m^3 for the present study; F_x and F_y are the aerodynamic drag and lift forces acting on the cylinder model in the x- and y-directions, respectively; C_{p_i} is the surface pressure coefficient on the cylinder model; p_i is the wall static pressure on the cylinder model; $i = 1–119$; p_∞ is the static pressure of the oncoming free stream upstream of the cylinder model; p_i and p_∞ are obtained from the digital pressure measurement system; θ_i is the pressure tap angle relative to the x-coordinate; and $\Delta\theta_i = 12^\circ$, where $\Delta\theta_i$ is the angle difference between two neighboring pressure taps.

The time histories and frequency spectra of the lift coefficients, C_y of the cylinder model at reduced velocities of 5.45, 5.96 and 6.86 are presented in Fig. 10. It can be seen clearly that, at the reduced velocity of 5.96, the time history of the lift coefficient had the largest oscillation amplitude and a well-defined dominant frequency of 5.61 Hz in the frequency spectrum. For the other test cases, the time histories of the lift coefficients are found to have much smaller VIV amplitudes. While the dominant frequency is still found to be 5.61 Hz for these cases, however, the power spectra are found to become much noisier compared with that of the case with reduced velocity of 5.96.

The rms values of the lift coefficients at different wind speeds are also analyzed, and the results are shown in Fig. 11. The results show that the changes of the rms values of the lift coefficients as a function of the reduced velocities is quite similar to that of the amplitudes of the cylinder vibrations described in Fig. 3. The largest rms value of the lift coefficients was found to appear in the 7$L/8$ section, and the smallest was in the 3$L/4$ section. It was also illustrated that the maximal fluctuating amplitude of the lift coefficient did not appear at the mid-span. This phenomenon may be induced by a three-dimensional flow surrounding the circular cylinder model, and the force coefficients were not correlated over the full cylinder length due to the finite length of the test model.

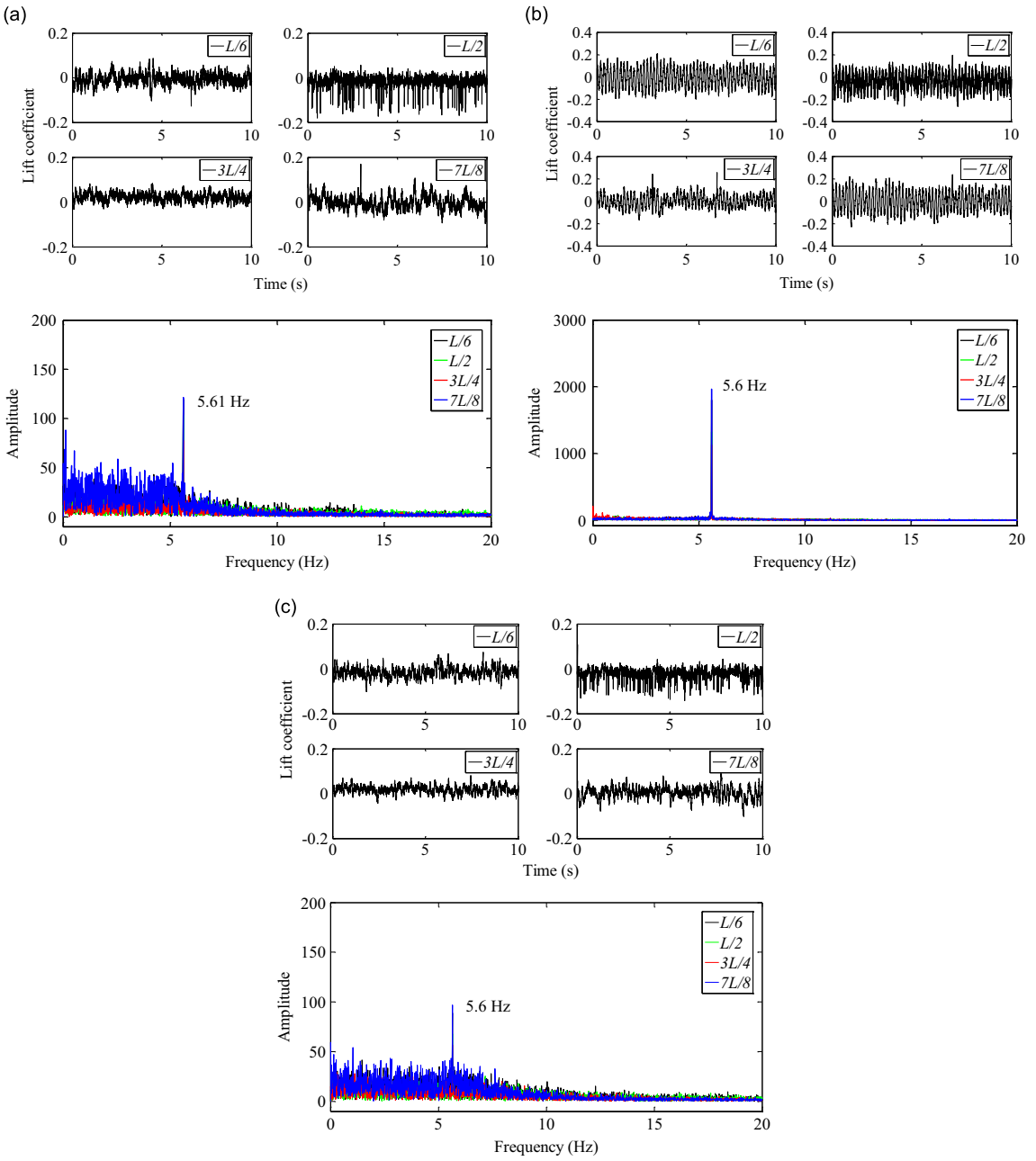

Fig. 10. Time histories and frequency spectra of the test model's lift coefficients for the cases with different reduced velocities: (a) 5.45, (b) 5.96 and (c) 6.86.

5.2. Suction control

Next, the lift coefficient of the circular cylinder with different suction flow velocities was studied. The lift coefficient at different sections of the circular cylinder model with suction flow control at the reduced velocity of 5.96 is shown in Fig. 12. The results with and without suction flow control are represented by the black and red dashed lines, respectively. It can be seen clearly that the suction control dramatically reduces the lift coefficient, with exception for the cases with suction flow rates of 16 ($C_\mu = 0.0021$) and 19 l/min ($C_\mu = 0.0030$) at $L/6$. The lift coefficient of this section under the larger suction flow rates of 16 ($C_\mu = 0.0021$) and 19 l/min ($C_\mu = 0.0030$) exhibited unsteady and larger rms values, which were induced by the larger pressure fluctuations, as shown in the right portion of Fig. 9(a).

The rms value of the lift coefficient versus wind speed is shown in Fig. 13. As shown in the figure, the lift coefficients had larger rms values for the cases with larger suction flow rates of 16 ($C_\mu = 0.0021$) and 19 l/min ($C_\mu = 0.0030$) at $L/6$. At the other three sections, the rms values of the lift coefficient for most of the other test cases are found

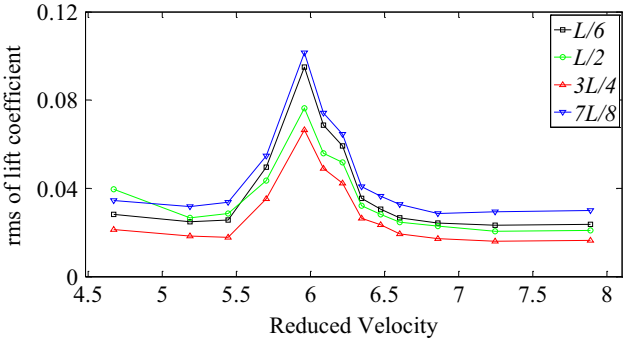

Fig. 11. rms of the lift coefficient at different reduced velocities.

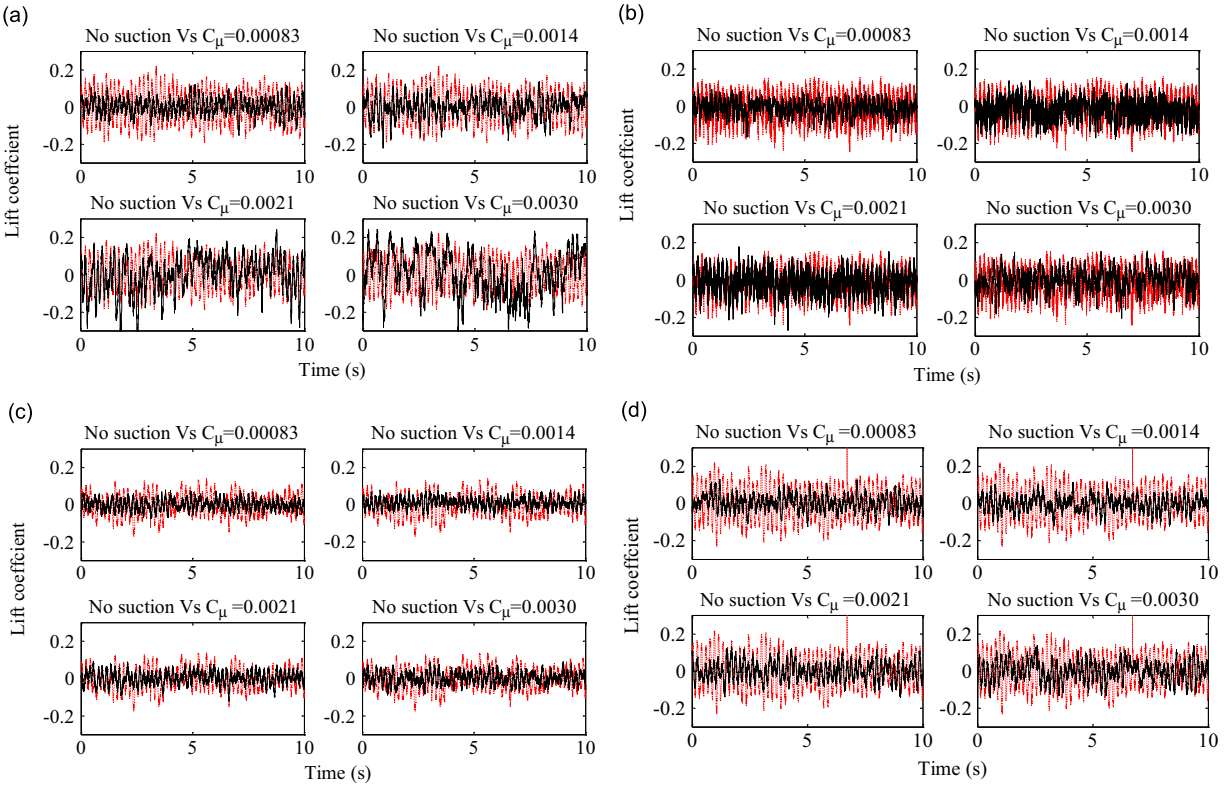

Fig. 12. Lift coefficient of the test model in different sections with suction flow control at a reduced velocity of 5.96: (a) $L/6$, (b) $L/2$, (c) 3 $L/4$ and (d) 7 $L/8$; the red lines denote the cases without suction control and the black lines denote those with suction control. (For interpretation of the references to color in this figure caption, the reader is referred to the web version of this article.)

to be smaller than those without suction flow control. Comparing the effects of suction flow control on the rms values of the lift coefficient with those of cylinder vibrations in Fig. 5, the vibration amplitudes are found to be the lowest for the case with the suction flow rate of 13 l/min ($C_\mu = 0.0014$), however, the rms value of the lift coefficient is found to be the smallest for the case with the suction flow rate of 10 l/min ($C_\mu = 0.00083$). For further investigation of the differences, the frequency spectra of the lift coefficient under the two flow rates were obtained, which are shown in Fig. 14. The rms values of the lift coefficient with the suction flow rate of 10 l/min ($C_\mu = 0.00083$) are found to be smaller than those of 13 l/min ($C_\mu = 0.0014$) case, but the maximum amplitudes of the lift coefficient in four sections with the suction flow rate of 10 l/min ($C_\mu = 0.00083$) are found to be larger than those of 13 l/min ($C_\mu = 0.0014$) case. As a result the case with the suction flow rate of 13 l/min ($C_\mu = 0.0014$) is found to have the lowest amplitude of the cylinder vibration.

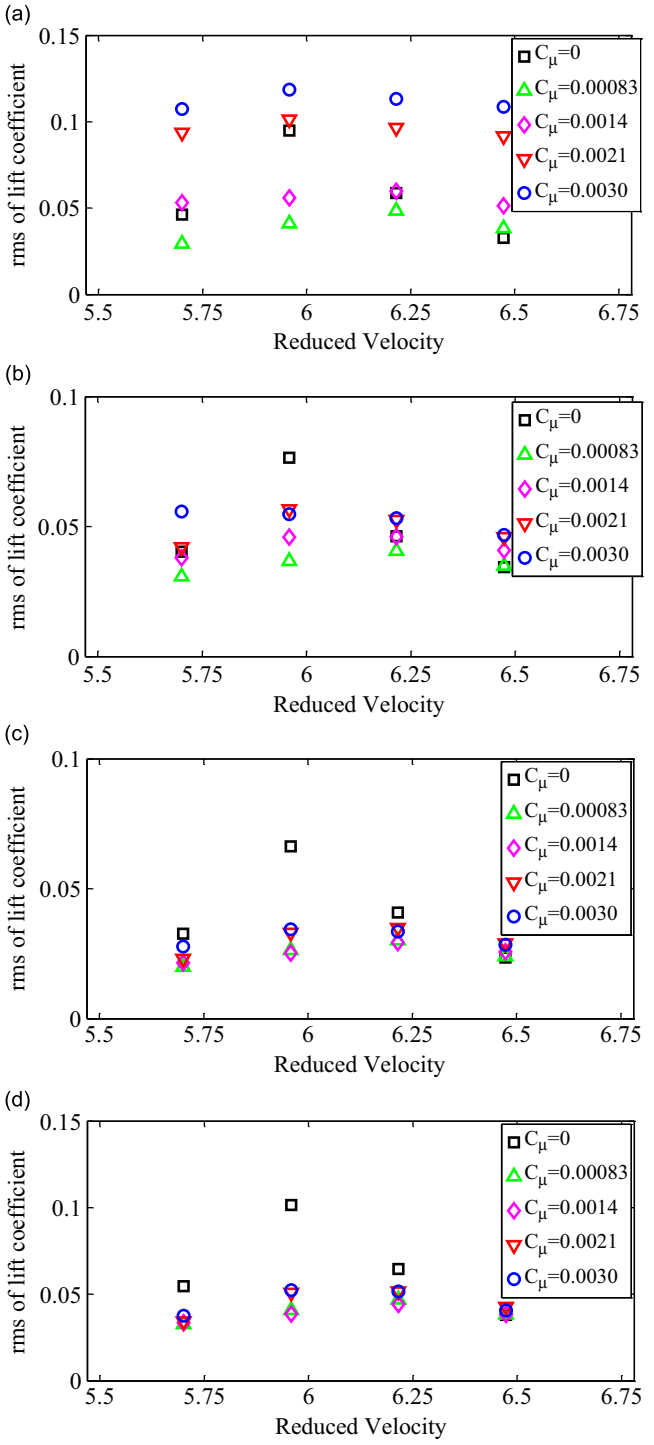

Fig. 13. rms values of the lift coefficient in different sections versus the reduced velocity: (a) $L/6$, (b) $L/2$, (c) $3L/4$ and (d) $7L/8$.

6. Discussion

As shown in Table 1, five suction velocities were adopted to control the flow field surrounding the circular cylinder. The velocity ratios of the suction velocity to the VIV starting velocity (6.11 m/s) are 0, 0.62, 0.80, 0.99 and 1.17 for the five tested cases. According to the analysis on cylinder oscillations, mean and fluctuating pressure distributions, and aerodynamic force coefficients described above, for the suction flow control approach as used in the present study, the

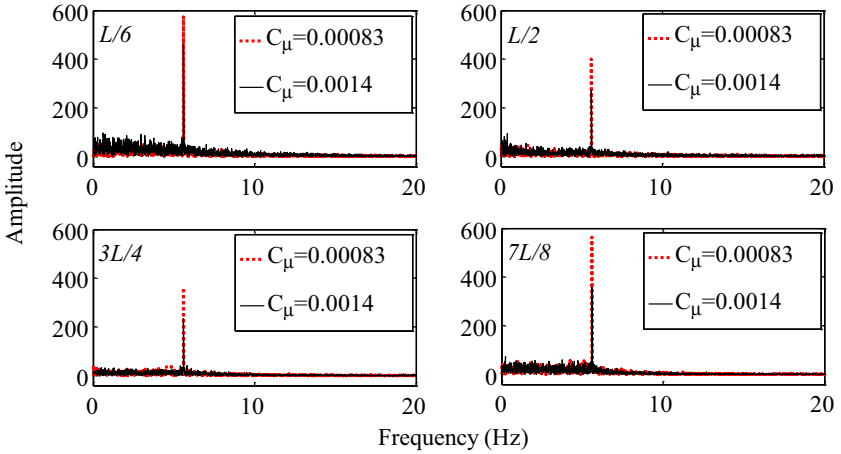

Fig. 14. Comparison of the frequency spectra of the lift coefficient.

control effectiveness is found to be better when the velocity ratio of the case is less than one. When the velocity ratio exceeds one, the control effectiveness is found to decrease with increasing suction flow rate.

Four pressure sections were employed to analyze the pressure distributions and aerodynamic forces acting on the test model. Based on the pressure distribution and aerodynamic coefficient results, the four sections are found to have similar trend when the velocity ratios of the test cases are less than one. However, the results at the $L/6$ cross section are found to be significantly different than those of the other three sections when the velocity ratio exceeded one (i.e., for the cases with suction flow rates of 16 ($C_\mu = 0.0018$–0.0023) and 19 l/min ($C_\mu = 0.0026$–0.0033)). The reason for this difference will be further investigated in the near future.

As we know, the VIV of the circular cylinder model is induced by the periodic fluctuating aerodynamic forces which are brought by the alternative shedding of the wake vortex and flow structures around the circular cylinder model. The purpose of the suction flow control is to break the alternating shedding process of the vortex structures, and the weakened vortex shedding will result in the reduction of the periodic fluctuating aerodynamic forces acting on the circular cylinder. According to the measurement results of the present study, it can be seen clearly that the suction flow control approach can reduce the fluctuating pressures and aerodynamic forces acting on the circular cylinder model effectively, thereby mitigating cylinder vibration, and controlling the VIV of the cylindrical cable model.

As demonstrated in the present study, the fluctuating pressures and aerodynamic forces are closely related to the flow field surrounding the circular cylinder model. In order to elucidate the fundamental mechanism of the suction flow control approach more clearly, advanced flow measurement techniques, such as particle image velocimetry (PIV), will be used in our future study to quantify the evolution of the unsteady vortex and turbulent flow structures surrounding the circular cylinder model. The effectiveness of the suction flow control method at different velocity ratios will be revealed more clearly and quantitatively based on whole-field measurements of the velocity and vorticity distributions around the circular cylinder.

7. Conclusion

In the present study, an experimental investigation was conducted to control/suppress the VIV of a circular cylinder by using a suction flow control method. The experimental study was conducted in a wind tunnel with a circular cylinder test model as a spring–mass system. The VIV of the test model with and without such flow control are quantified in the terms of the dynamics of the vibration responses, the mean and fluctuating pressure coefficients, and the aerodynamic force coefficients acting on the test model. Important flow parameters, such as the reduced velocity of the oncoming flow and the suction flow rate, on the effectiveness of the suction control method to suppress VIV of the test model are assessed quantitatively.

The measurement results indicate clearly that the suction flow control method exhibits excellent control performance to suppress the VIV of the test model by substantially reducing the amplitude of the VIV oscillation, fluctuating surface pressure, and the unsteady aerodynamic forces acting on the test model. By comparing the test cases with different suction flow rates, it is found that there exists an optimal suction flow rate for the best VIV control. The cases with higher suction flow rates do not necessarily behave better than those with lower suction flow rates. The suction flow control method is found to have the best control effectiveness for VIV suppression when the velocity ratio of the suction flow velocity to the oncoming free stream flow velocity to start the VIV of the test model is less than one.

It should be noted that, as the first report of an ongoing multi-year research project, the major objective of the present study is to demonstrate the effectiveness of using suction flow method to control/suppress VIV phenomena. While the time-resolved measurement results reported in the present study, in the terms of the dynamics of the vibration responses,

the mean and fluctuating pressure coefficients, and the resultant aerodynamic force coefficients acting on the test model, are very useful and essential to reveal many interesting features and important global characteristics of the VIV phenomena with and without suction flow control. It is highly desirable to obtain the quantitative information about the corresponding flow field around the test model in order to elucidate the underlying physics of the VIV phenomena more clearly. With this goal in mind, we are conducting detailed flow field measurements by using a high-resolution Particle Image Velocimetry (PIV) system to quantify the time evolution of the unsteady vortex and wake flow structures around the test model with and without suction flow control. The detailed flow field measurement results will be reported in our future papers.

Acknowledgments

This research was funded by the National Natural Sciences Foundation of China (NSFC) (90815022, 51161120359, 51008093, 50908069 and 51008103) and the Fundamental Research Funds for the Central Universities (HIT. NSRIF. 2009099).

References

Amitay, M., Honohan, A., Trautman, M., Glezer, A., 1997. Modification of the Aerodynamic Characteristics of Bluff Bodies using Fluidic Actuators. AIAA Paper No., 97–2004.
Amitay, M., Smith, B.L., Glezer, A., 1998. Aerodynamic flow Control using Synthetic Jet Technology. AIAA Paper No., 98–0208.
Arcas, D., Redekopp, L., 2004. Aspects of wake vortex control through base blowing/suction. Physics of Fluids 16, 452–456.
Baban, E., So, R.M.C., 1991. Aspect ratio effect on flow-induced forces on circular cylinders in a cross-flow. Experiments in Fluids 10, 313–321.
Bao, Y., Tao, J., 2013. The passive control of wake flow behind a circular cylinder by parallel dual plates. Journal of Fluids and Structures 37, 201–219.
Bernitsas, M.M., Raghavan, K., Ben-Simon, Y., Garcia, E.M.H., 2008. VIVACE (Vortex Induced Vibration Aquatic Clean Energy): a new concept in generation of clean and renewable energy from fluid flow. Journal of Offshore Mechanics and Arctic Engineering 130. 041101-1–15.
Chng, T.L., Rachman, A., Tsai, H.M., Zha, G.C., 2009. Flow control of an airfoil via injection and suction. Journal of Aircraft 46 (1), 291–300.
Delaunay, Y., Kaiktsis, L., 2001. Control of circular cylinder wakes using base mass transpiration. Physics of Fluids 13, 3285–3302.
Farivar, D., 1981. Turbulent uniform flow around cylinders of finite length. AIAA Journal 19 (3), 275–281.
Feng, L.H., Wang, J.J., Pan, C., 2010. Effect of novel synthetic jet on wake vortex shedding modes of a circular cylinder. Journal of Fluids and Structures 26, 900–917.
Feng, L.H., Wang, J.J., 2010. Circular cylinder wake vortex synchronization control with synthetic jet positioned at back stagnation point. Journal of Fluid Mechanics 662, 232–259.
Feng, L.H., Wang, J.J., Pan, C., 2011. Proper orthogonal decomposition analysis of vortex dynamics of a circular cylinder under synthetic jet control. Physics of Fluid 23. 014106-1–13.
Flamand, O., 1995. Rain-wind-induced vibration of cables. Journal of Wind Engineering and Industrial Aerodynamics 57, 353–362.
Fransson, J.H.M., Alfredsson, P.H., 2003. On the disturbance growth in an asymptotic suction boundary layer. Journal of Fluid Mechanics 482, 51–90.
Fransson, J.H.M., Konieczny, P., Alfredsson, P.H., 2004. Flow around a porous cylinder subject to continuous suction or blowing. Journal of Fluids and Structures 19, 1031–1048.
Gbadebo, S.A., Cumpsty, N.A., Hynes, T.P., 2008. Control of three-dimensional separations in axial compressors by tailored boundary layer suction. Journal of Turbomachinery 130 (011004), 1–8.
Grager, T., Rothmayer, A., Hu, H., 2011. Stall suppression of a low-Reynolds-number airfoil with a dynamic burst control plate. In: 49th AIAA Aerospace Sciences Meeting including the New Horizons Forum and Aerospace Exposition, AIAA 2011–1180, Orlando, Florida.
Greenblatt, D., Paschal, K.B., Yao, C.S., Harris, J., Schaeffler, N.W., Washburn, A.E., 2006. Experimental investigation of separation control part 1: baseline and steady suction. AIAA Journal 44 (12), 2820–2830.
Skop, R.A., Balasubramanian, R., 1997. A new twist on an old model for vortex-excited vibrations. Journal of Fluids and Structures 11, 395–412.
Gu, M., Du, X.Q., 2005. Experimental investigation of rain–wind-induced vibration of cables in cable-stayed bridges and its mitigation. Journal of Wind Engineering and Industrial Aerodynamics 93, 79–95.
Hikami, Y., Shiraishi, N., 1988. Rain-wind induced vibrations of cables in cable stayed bridges. Journal of Wind Engineering and Industrial Aerodynamics 29, 409–418.
Korkischko, I., Meneghini, J.R., 2012. Suppression of vortex-induced vibration using moving surface boundary-layer control. Journal of Fluids and Structures 34, 259–270.
Li, H., Liu, M., Li, J.H., Guan, X.C., Ou, J.P., 2007. Vibration control of stay cables of the Shandong Binzhou Yellow River Highway Bridge by using magnetorheological fluid dampers. ASCE, Journal of Bridge Engineering, 12; 401–409.
Li, Z., Navon, I., Hussaini, M., Le Dimet, F., 2003. Optimal control of cylinder wakes via suction and blowing. Computers & Fluids 32, 149–171.
Liu, M., Song, G.B., Li, H., 2007. Non-model-based semi-active vibration suppression of stay cables using magneto-rheological fluid damper. Smart Materials and Structures 16, 1447–1452.
Main, J. A. and Jones, N. P., 1999. Full-scale measurements of stay cable vibration. In: 10th International Conference on Wind Engineering (10ICWE). Wind Engineering into the 21st century, vol. 1–3, pp. 963–970.
Main, J.A., Jones, N.P., 2001. Evaluation of viscous dampers for stay-cable vibration mitigation. ASCE, Journal of Bridge Engineering, 6; 385–397.
Matsumoto, M., Shiraishi, N., Shirato, H., 1992. Rain-wind induced vibration of stay-cables of cable-stayed bridges. Journal of Wind Engineering and Industrial Aerodynamics 41-44, 2011–2022.
Matsumoto, M., Shirato, H., Yagi, T., Goto, M., Sakai, S., Ohya, J., 2003. Field observation of the full-scale wind-induced cable vibration. Journal of Wind Engineering and Industrial Aerodynamics 91, 13–26.
Modi, V.J., 1997. Moving surface boundary-layer control: a review. Journal of Fluids and Structures 11, 627–663.
Munshi, S.R., Modi, V.J., Yokomizo, T., 1997. Aerodynamics and dynamics of rectangular prisms with momentum injection. Journal of Fluids and Structures 11, 873–892.
Oruç, V., 2012. Passive control of flow structures around a circular cylinder by using screen. Journal of Fluids and Structures 33, 229–242.
Owen, J.C., Bearman, P.W., 2001. Passive control of VIV with drag reduction. Journal of Fluids and Structures 15, 597–605.
Patil, S.K.R., Ng, T.T., 2010. Control of separation using spanwise periodic porosity. AIAA Journal 48 (1), 174–187.
Patnaik, B.S.V., Wei, G.W., 2002. Controlling wake turbulence. Physical Review Letters 88, 35–40.
Persoon, A. J. Noorlander, K., 1999. Full scale measurements on the Erasmus Bridge after rain/wind induced cable vibration, in: A. Larsen, G.L. Larose, F.M. Livesey (Eds.), Proceedings of the 10th International Conference On Wind Engineering, Copenhagen, Denmark, 21–24, 1019–1026.
Qin, N., Zhu, Y., Poll, D.I.A., 1998. Surface suction on aerofoil aerodynamic characteristics at transonic speeds. Proceedings of the Institution of Mechanical Engineers, Part G: Journal of Aerospace Engineering 212 (5), 339–351.

Qiu, Y., 2010. Characteristics of Wind Loads on Spherical Shells with Large Rise-span Ratio. Dissertation for the Master Degree, 6-20. Harbin Institute of Technology, Harbin, China.
Sakamoto, H., Arie, M., 1983. Vortex shedding from a rectangular prism and a circular cylinder placed vertically in a turbulent boundary layer. Journal of Fluid Mechanics 126, 147–165.
Seal, C.V., Smith, C.R., 1999. The control of turbulent end-wall boundary layers using surface suction. Experiments in Fluids 27, 484–496.
Tchieu, A.A., Leonard, A., 2012. Experimental investigation on the suppression of vortex-induced vibration of long flexible riser by multiple control rods. Journal of Fluids and Structures 30, 115–132.
Tensi, J., Boué, I., Paillé, F., Dury, G., 2002. Modification of the wake behind a circular cylinder by using synthetic jets. Journal of Visualization 5, 37–44.
Wang, L.Y., Xu, Y.L., 2007. Active stiffness control of wind-rain-induced vibration of prototype stay cable. International Journal for Numerical Methods in Engineering 74 (1), 80–100.
Wu, C.J., Wang, L., Wu, J.Z., 2007. Suppression of the von Karman vortex street behind a circular cylinder by a traveling wave generated by a flexible surface. Journal of Fluid Mechanics 574, 365–391.
Wu, H., Sun, D.P., Lu, L., Teng, B., Tang, G.Q., Song, J.N., 2012. Experimental investigation on the suppression of vortex-induced vibration of long flexible riser by multiple control rods. Journal of Fluids and Structures 30, 115–132.
Zdravkovich, M.M., Brand, V.P., Mathew, G., Weston, A., 1989. Flow past short circular cylinders with two free ends. Journal of Fluid Mechanics 203, 557–575.
Zhou, H.J., Xu, Y.L., 2007. Wind–rain-induced vibration and control of stay cables in a cable-stayed bridge. Structural control and health monitoring 14, 1013–1033.
Zuo, D., Jones, N.P., Main, J.A., 2008. Field observation of vortex- and rain-wind-induced stay-cable vibrations in a three-dimensional environment. Journal of Wind Engineering and Industrial Aerodynamics 96, 1124–1133.
Zuo, D., Jones, N.P., 2010. Interpretation of field observations of wind- and rain-wind-induced stay cable vibrations. Journal of Wind Engineering and Industrial Aerodynamics 98, 73–87.